JAST (Journal of Animal Science and Technology) TITLE PAGE

Upload this completed form to website with submission

ARTICLE INFORMATION	Fill in information in each box below
Article Type	Research article
Article Title (within 20 words without abbreviations)	Garlic oil and rubber seed oil mixtures modulate rumen fermentation and microbiome for methane mitigation in vitro
Running Title (within 10 words)	Garlic-rubber seed oils modulate rumen microbiome and methane
Author	Mekonnen Tilahun1, Jongsik Jeong1, Geonwoo Kim1, Ryukseok Kang1, Wanho Jo1, Myeong-Gwan Oh1, Chaemin Yu1, Changbeen Jang1, Gihwal Son2, Jaeyong Song3, Tansol Park1,*
Affiliation	1 Department of Animal Science and Technology, Chung-Ang University, Anseong-si 17546, Republic of Korea 2 Nonghyup Livestock Research Center, Anseong-si 17558, Republic of Korea 3 Nonghyup Feed Co., LTD., Seoul 05398, Republic of Korea
ORCID (for more information, please visit https://orcid.org)	Mekonnen Tilahun (https://orcid.org/0000-0001-9894-2562) Jongsik Jeong (https://orcid.org/0009-0002-8660-5598) Geonwoo Kim (https://orcid.org/0009-0003-8080-5860) Ryukseok Kang (https://orcid.org/0009-0001-6202-1283) Wanho Jo (https://orcid.org/0009-0006-9607-550X) Myeong-Gwan Oh (https://orcid.org/0009-0007-2021-0143) Chaemin Yu (https://orcid.org/0009-0000-6275-800X) Changbeen Jang (https://orcid.org/0009-0007-9771-5342) Gihwal Son (https://orcid.org/0000-0001-6406-0262) Jaeyong Song (https://orcid.org/0000-0002-8613-5605) Tansol Park (https://orcid.org/0000-0002-4480-4524)
Competing interests	Authors Gihwal Son and Jaeyong Song were employed by the Nonghyup Livestock Research Center and Nonghyup Feed Co., Ltd., respectively. The remaining authors declare that the research was conducted in the absence of any commercial or financial relationships that could be construed as a potential conflict of interest.
Funding sources State funding sources (grants, funding sources, equipment, and supplies). Include name and number of grant if available.	This research was supported by the Hanwoo research project (2024) of the Nonghyup Feed Co., Ltd.
Acknowledgements	The research was supported by the Chung–Ang University Graduate Research Scholarship (Academic scholarship for the College of Biotechnology and Natural Resources) in 2025.

Availability of data and material	The datasets generated in this study are available in online repositories. The repository name(s) and corresponding accession number(s) can be accessed in the NCBI database: https://www.ncbi.nlm.nih.gov/bioproject/PRJNA1377940.
Authors' contributions Please specify the authors' role using this form.	Conceptualization: Tilahun M, Park, T. Data curation: Tilahun M, Jeong J, Park T. Formal analysis: Tilahun M, Park T. Methodology: Tilahun M, Jeong J, Kim G, Kang R, Jo W, Oh M-G, Yu C, Jang C. Software: Tilahun M, Park T. Validation: Jeong J, Kim G, Kang R, Jo W, Oh M-G, Yu C, Jang C, Son G, Song J. Investigation: Tilahun M, Park T. Writing - original draft: Tilahun M. Writing - review & editing: Jeong J, Kim G, Kang R, Jo W, Oh M-G, Yu C, Jang C, Son G, Song J, Park T.
Ethics approval and consent to participate	The procedures were approved by the Institutional Animal Care and Use Committee (IACUC) at Chung-Ang University (202401030036) and followed all ethical standards outlined in the IACUC's animal welfare guidelines.

CORRESPONDING AUTHOR CONTACT INFORMATION

For the corresponding author (responsible for correspondence, proofreading, and reprints)	**Fill in information in each box below**
First name, middle initial, last name	Tansol Park
Email address – this is where your proofs will be sent	tansol@cau.ac.kr
Secondary Email address	tansol1719@gmail.com
Address	Department of Animal Science and Technology, Chung-Ang University, Anseong-si 17546, Gyeonggi-do, Republic of Korea
Cell phone number	
Office phone number	+82-31-670-3256
Fax number	+82-31-675-3108

Garlic oil and rubber seed oil mixtures modulate rumen fermentation and microbiome for methane mitigation *in vitro*

Mekonnen Tilahun[1], Jongsik Jeong[1], Geonwoo Kim[1], Ryukseok Kang[1], Wanho Jo[1], Myeong-Gwan Oh[1], Chaemin Yu[1], Changbeen Jang[1], Gihwal Son[2], Jaeyong Song[3], Tansol Park[1,*]

[1] Department of Animal Science and Technology, Chung-Ang University, Anseong-si 17546, Republic of Korea

[2] Nonghyup Livestock Research Center, Anseong-si 17558, Republic of Korea

[3] Nonghyup Feed Co., LTD., Seoul 05398, Republic of Korea

*** Correspondence**

Tansol Park

tansol@cau.ac.kr

Abstract (up to 350 words)

Ruminant methane emissions account for approximately 14.5% of anthropogenic greenhouse gas emissions, underscoring the need for microbiome-targeted mitigation strategies that preserve fermentation efficiency. This *in vitro* rumen fermentation study evaluated garlic oil (GO; 0.03% v/v), rubber seed oil (RO; 2–6% substrate v/v), and their combination (GORO) on fermentation, methanogenesis, and microbial ecology using 16S rRNA gene sequencing and PICRUSt2 functional predictions (n=5 replicates/treatment). The GO and GORO treatments reduced methane yield by ~50% (3.21–3.66 mL vs. 6.54–7.11 mL in control (CON)/RO; $p < 0.001$) and decreased the dry matter digestibility (64.1–66.8% vs. 68.5–70.7%; $p < 0.001$). Volatile fatty acid (VFA) profiles shifted toward propionate (21.2–21.6 vs. 19.6–19.9 mol/100 mol; $p < 0.001$), and reduced the acetate to propionate ratios (2.72–2.77 vs. 3.12–3.19; $p < 0.001$), while total VFA remained unchanged ($p = 0.08$). Microbial analyses revealed that GO induced alpha diversity loss (Chao1: 865 vs. 1,257 in CON; $p < 0.05$), but GORO restored richness (Chao1:1,256) and enriched cellulolytics (*Ruminococcus* 8.2% vs. 2.1%; *Fibrobacter* 1.9% vs. 0.45%). For GO, methanogenesis suppression was associated with a 76% decline in *Methanobrevibacter* ($p < 0.001$) and a 5.6–fold rise in *Selenomonas* ($p < 0.001$). Functional predictions showed GO upregulated methylmalonyl-CoA decarboxylase, and GORO restored endo-1,4-β-xylanase activity. Random Forest classification identified *Selenomonas* as the top biomarker, and network analysis linked *Clostridium* to methanogenesis ($\rho = 0.85$ with CH_4; $p < 0.001$). These findings support the use of phytogenic oils as biotechnological tools to redirect hydrogen toward sustainable pathways while preserving microbial ecosystem stability.

Keywords: Methane mitigation; Garlic oil; Rubber seed oil; Rumen microbiome; Metabolic reprogramming; Microbial biomarkers

Introduction

Enteric methane emissions from ruminants account for approximately 14.5% of global greenhouse gas emissions and cause energy losses of up to 12% of gross intake (1, 2). Developing mitigation strategies for methane emissions that do not compromise productivity or rumen health is a primary priority.

Research on mitigating methane emissions has primarily focused on dietary interventions, feed additives, vaccines, and selective breeding (3-5). Among natural alternatives, essential oils (EOs) are promising because of their antimicrobial properties and their ability to alter rumen fermentation, decrease methane emissions, and enhance nutrient utilization (6-8).

This study investigates plant–derived oil that exhibits distinct bioactive profiles, such as garlic oil (GO), which is abundant in organosulfur compounds, inhibits methanogens and protozoa, diminishes methane emissions, and alters volatile fatty acid (VFA) profiles; however, it is noteworthy that high dosages may adversely affect fiber digestion and microbial diversity (9-11).

Rubber seed oil (RO), extracted from *Hevea brasiliensis*, is abundant in polyunsaturated fatty acids (PUFAs), including linoleic acid (C18:2) and α-linolenic acid (C18:3), which constitute up to 50-60% of its fatty acid profile and can enhance the nutritional quality of associated products (12, 13). PUFAs from plant oils have been shown to modulate rumen fermentation by serving as alternative hydrogen sinks during biohydrogenation, exerting direct antimicrobial effects on methanogenic archaea and protozoa, and shifting VFA production toward propionate, which can reduce methane output (14, 15). While RO has demonstrated improvements in nutrient digestibility and rumen fatty acid profiles in dairy cows(13, 16), its direct influence on rumen fermentation and methane generation, especially when combined with other bioactive compounds, is poorly understood. Integrating diverse bioactive constituents to explore potential synergistic or antagonistic effects is a

validated and strategic approach to overcoming these challenges and enhancing overall treatment efficacy and stability.

We hypothesized that (1) GO would reduce methane emission by inhibiting methanogens and protozoa, (2) RO would independently reduce methane emissions through biohydrogenation of its PUFAs and modulation of rumen microbes, though its standalone effects may be limited compared to more targeted antimicrobials; and (3) the combination of GO and RO would synergistically lower methane emissions by combining organosulfur inhibition with PUFA mediated biohydrogenation, potentially at lower doses to minimize adverse effects on rumen function. To test these hypotheses, we conducted an integrated *in vitro* fermentation experiment and performed fermentation parameter analyses, microbial quantification, and 16S rRNA gene sequencing to explore the individual and combined effects of these treatments and identify microbial taxa and predicted functional pathways associated with methane reduction.

Materials and Methods

Experimental design and treatments

An *in vitro* rumen fermentation experiment was conducted to evaluate the effects of GO and RO, both individually and in combination, on fermentation characteristics and microbial community dynamics. Eight dietary treatments were evaluated: a control group (CON) with no additives, RO added at 2%, 4%, and 6% v/v (RO2, RO4, and RO6, respectively), GO at 0.03% v/v, and combined treatments of GO with RO at each of the RO levels (GORO2, GORO4, and GORO, respectively). The GO concentration was selected based on preliminary studies and literature reports indicating optimal anti-methanogenic activity without complete fermentation inhibition (10, 17, 18). RO concentrations were selected based on practical supplementation levels for lipid-rich oils in ruminant nutrition, enabling dose-dependent evaluation without adverse effects on palatability or health. This range aligns with *in vitro* studies on vegetable oils for methane mitigation, where minimum effective

concentrations for reductions in methanogenesis and VFA shifts start at ~2%, with stronger effects at 4-6% (13, 19-21) that would not negatively impact feed palatability or animal health performance.

Rumen fluid collection and preparation

Rumen fluid was collected from three Hanwoo cows at the Nonghyup Co., Ltd. research farm, located about 30 min from our lab. The procedures were approved by the Institutional Animal Care and Use Committee (IACUC) at Chung-Ang University (202401030036) and followed all ethical standards outlined in the IACUC's animal welfare guidelines. The cows were fasted for 12 h before collecting rumen fluid to ensure consistent baseline conditions. Rumen fluid was obtained using a vacuum pump system, stored in an airtight, insulated container prefilled with 99.999% CO_2, and directly transported to the laboratory within 30 min.

***In vitro* fermentation procedure**

In vitro fermentation was conducted according to the method described by Goering and Van Soest (22). Briefly, upon arrival at the laboratory, the rumen fluid was filtered through two layers of cheesecloth to remove particulate impurities and then combined with buffer solution at twice its volume. The pH was subsequently measured and adjusted to 6.7 using CO_2 buffering. The inoculum was continuously flushed with oxygen-free CO_2 to maintain anaerobic conditions. The experimental substrate, which was identical to the feed used at the research farm (Table 1), was ground to pass through a 1–mm screen and oven-dried at 55℃ for 48 h prior to placement in the fermentation vessels. Each 125 mL fermentation vessel was loaded with 500 mg of substrate, which consisted of a 1:1 mixture of oat hay and pelleted commercial concentrate (Nonghyup Co., Ltd. research farm), along with 50 mL of the prepared inoculum (McDougall's buffer and filtered rumen fluid in a 2:1 v/v ratio). Treatment additives were incorporated into the substrate prior to inoculation. The fermentation vessels were sealed under anaerobic conditions via CO_2 flushing and incubated at 39°C and 60 rpm for 24 hours.

Five replicate vessels were prepared for each treatment. pH was measured after 24 h of incubation using a calibrated digital pH meter (MW150, Milwaukee Instruments, Inc., Rocky Mount, NC, USA) with standard buffer solutions.

Fermentation parameter analysis

Gas production measurements: The headspace gas pressure within the fermentation vessel was measured using a pressure transducer (L20000DCV3, Laurel Electronics, Inc., Costa Mesa, CA, USA). Concurrently, gas was collected in a gas bag using a rubber stopper, a needle, and a three-way cock setup (23). Gas pressure measurements were performed at 3, 6, 12, and 24 h during incubation, with continuous monitoring to ensure that pressures did not exceed 480 mbar, as excessive pressure can suppress microbial activity and alter fermentation outcomes (24). The gas volume was estimated by converting pressure readings from mbar to milliliters using a calibration procedure involving the injection of air into a similarly sized fermentation vessel filled with distilled water and an equivalent volume of inoculum, under standard atmospheric conditions (23).

The methane concentration was measured using a gas chromatography system (YL6500 GC, Youngin Chromass, Anyang, Republic of Korea), equipped with a thermal conductivity detector and a packed GC column (G359180055, Agilent Technologies Inc., Santa Clara, CA, USA). A gas-tight syringe (1010 TLL, Hamilton, Reno, NV, USA) was used for injection. CH_4 levels were measured in duplicate within two days of collection.

Volatile fatty acid analysis: VFA samples were prepared by centrifuging 1.8 mL of the inoculum at 16,000 × *g* for 15 min at 4°C. Subsequently, 1.0 mL of the supernatant was combined with 0.2 mL of 25% (w/v) metaphosphoric acid and stored at 80°C until analysis. The quantification of VFAs, including acetate, propionate, butyrate, iso-butyrate, valerate, and iso-valerate, was conducted using a gas chromatography (model 7890B, Agilent Technologies, Santa Clara, CA, USA) equipped with an autosampler (7693A, Agilent Technologies), a flame ionization detector, and a Nukol fused silica capillary column (Supelco, Bellefonte, PA, USA).

Ammonia nitrogen determination: Ammonia nitrogen (NH_3N), samples were prepared by centrifuging 1.8 mL of the inoculum at 16,000 *g* for 15 min at 4°C. Then, 0.5 mL was combined with 0.1 mL of 0.2 M sulfuric acid (H_2SO_4) and stored at 4°C until further analysis. The concentration of NH_3N was quantified using a microplate spectrophotometer (INNO, LTEK, Seongnam, Republic of Korea), following the colorimetric method of Chaney and Marbach (25) with modifications introduced by Hamid, Moon (26). Ammonium chloride was used as the standard reference.

Dry matter digestibility: *In vitro* dry matter digestibility (DMD) was measured gravimetrically by weighing the remaining substrate after a 24 h fermentation period. The fermentation contents were filtered through a preweighed F57 filter bag (Ankom Technology, Macedon, NY, USA), dried at 65°C for 72 h, and then weighed to determine the digestibility percentage.

Microbial abundance analysis

Quantitative PCR analysis: Microbial pellets that remained after centrifuging the inoculum samples to generate VFA samples were stored at 80°C until DNA extraction was performed. Metagenomic DNA was extracted from the pellets of all samples using the RBB+C method described by Yu and Morrison (27). The concentration and purity of the extracted DNA were assessed using a Nanodrop One Microvolume UV-Vis Spectrophotometer (Thermo Fisher Scientific, Waltham, MA, USA). The absolute abundance of key microbial populations, including total bacteria and methanogens, was determined using quantitative PCR (qPCR) with universal primers specific to each microbial group, and results were presented as log copies/mL of inoculum.

Each qPCR reaction consisted of 1 μL of template DNA combined with 15 μL of reaction mixture containing 0.075 μL of each primer (forward and reverse, each at 100 μM), 7.5 μL of PowerUp SYBR Master Mix (2X), and 6.35 μL of ultrapure water. The qPCR amplification procedures adhered to protocols optimized for each primer set to ensure precise and reproducible results. The thermal cycling protocol consisted of an initial denaturation phase at 95°C lasting for 3 min, followed by 40 cycles of denaturation at 95°C for 15 s, annealing at 60°C for 30 s, and extension at 72°C for 30 s.

Protozoal enumeration. Rumen protozoa were quantified through direct microscopy utilizing an enhanced Neubauer hemocytometer after fixation with an 18.5% formaldehyde solution. Samples were diluted 1:10 with saline, and total protozoa, entodiniomorphs, and isotrichids were enumerated and expressed as $\log_{10}$ cells/mL.

16S rRNA gene sequencing and bioinformatics

DNA extraction and library preparation. For a detailed understanding of the microbial ecology of the CON, GO, and GORO treatments, 16S rRNA gene sequencing was performed explicitly on the treatment samples. Each treatment was conducted with five replicates to ensure the statistical reliability and robustness of the data. Total DNA was extracted from the fermentation fluid samples using the Bioneer AccuPrep Genomic DNA Extraction Kit (Bioneer, Daejeon, Republic of Korea) following the manufacturer's protocols. DNA quality and concentration were assessed using a NanoDrop 2000 spectrophotometer (Thermo Fisher Scientific) and Qubit 4.0 fluorometer (Invitrogen, Carlsbad, CA).

The V3-V4 hypervariable regions of the bacterial 16S rRNA gene were amplified using primers 341F (5'CCTACGGGNGGCWGCAG3') and 805R (5'GACTACHVGGGTATCTAATCC3') [28]. These amplicons were sequenced using an Illumina MiSeq PE300 platform (Illumina, San Diego, United States). The standard protocols of Majorbio BioPharm Technology Co., Ltd. in Shanghai, China, were followed.

Sequence processing and analysis: The initial microbiome analysis was conducted using Quantitative Insights into Microbial Ecology Version 2 (QIIME2) (29), which processed 16S rRNA sequences. Cutadapt (30) was employed to remove primer sequences, and then the DADA2 plugin (31) was applied for quality control ($Q \geq 25$), denoising, merging, and chimera removal. Chimeric sequences were removed using the consensus method, and taxonomy was assigned against the SILVA 138 database (32, 33), which had been pretrained using the Naïve Bayes algorithm(34). Any amplicon sequence variants (ASVs) that were unassigned or associated with mitochondria, chloroplasts, or archaea were excluded. The ASV table in BIOM format and corresponding

representative sequences were then utilized for subsequent analyses. In this study, only taxa present in all samples from at least one treatment group were discussed.

Microbial diversity analysis encompassed alpha-diversity metrics, such as Chao1, Simpson, Shannon, and Faith's phylogenetic diversity, and was processed in QIIME2 (29). Beta diversity was assessed using Bray-Curtis dissimilarity matrices and visualized through Principal Coordinates Analysis (PCoA). Permutational Multivariate Analysis of Variance (PERMANOVA) was performed to test for significant differences in microbial community structure among treatments using the vegan package in R (35).

Functional profiling

Functional potential of microbial communities was predicted using PICRUSt2 (Phylogenetic Investigation of Communities by Reconstruction of Unobserved States) (36). Enzyme Commission (EC) numbers were extracted and filtered based on minimum abundance thresholds (≥ 0.01% mean relative abundance).

Statistical analysis of fermentation traits and microbial abundances

All statistical analyses were conducted using R (version 4.4.0). Data normality was assessed using Shapiro-Wilk tests, and homogeneity of variance was evaluated using Levene's test. For parametric data, one-way ANOVA followed by Tukey's Honestly Significant Difference (HSD) post hoc test was used for multiple comparisons. Nonparametric data were analyzed using the Kruskal-Wallis test followed by Dunn's test with the Benjamini-Hochberg (BH) correction for multiple comparisons.

Microbial abundance data were analyzed using nonparametric approaches due to their compositional nature and nonnormal distributions. Differential abundance analyses of microbial genera were performed using Kruskal-Wallis tests with Benjamini–Hochberg (BH)–adjusted *p*-values. The dependent variable was the relative abundance of each genus, compared across experimental groups (CON vs GO, CON vs GORO, and GO vs GORO). Only genera with a mean relative abundance ≥ 0.01% were used for visualization and statistical inference. Analyses were conducted using the phyloseq package (37), with graphical outputs generated in ggplot2 (38) and pheatmap (39). The

differential abundance and functional expression analysis were performed using DESeq2 (40). For microbial taxa, the dependent variable was the normalized read count per genus, compared across experimental conditions (CON vs GO, CON vs GORO, and GO vs GORO). For functional analysis, DESeq2 was applied to enzyme commission (EC) numbers, where the dependent variable was the normalized abundance of genes annotated to each EC category. Stringent significance criteria were applied: an adjusted p-value < 0.01 and an absolute $\log_2$ fold change ($|\log_2 FC|$) > 2. Statistical significance was set at $p < 0.05$ for all analyses unless otherwise specified. The results are reported as means ± pooled standard error of the mean (SEM) with appropriate statistical annotations.

Multivariate and correlation analysis

Principal Component Analysis (PCA) was performed on scaled microbial abundance data using the prcomp() function in R to visualize the overall treatment effects on the microbial community structure. PCA biplots were generated using the factoextra package (41) to illustrate how individual traits contributed to the PCA axes. Spearman's rank correlation was employed to assess the relationships among fermentation traits and microbial genera and, the complex interdependencies within the rumen ecosystem.

Correlation networks between microbial genera and fermentation traits were constructed using Spearman's rank correlation with significance thresholds of $|\rho| > 0.70$ and $p < 0.05$ (Benjamini-Hochberg adjusted). Network topology was analyzed using the igraph package (42) and ggraph (43) to identify hub taxa and central nodes based on degree and betweenness centrality measures.

Machine learning and biomarker identification

Random Forest classification. Machine learning approaches were applied to identify microbial biomarkers distinguishing treatment groups using the randomForest package (44). Feature importance was assessed using the Mean Decrease Accuracy and Mean Decrease Gini metrics. Model performance was evaluated using out-of-bag (OOB) error rates and cross–validation.

Feature selection algorithms: The rfPermute package was used to assess the statistical significance of feature importance through permutation testing (45). Boruta feature selection was employed to

identify robust and, nonrandom predictors by comparing feature importance against shadow variables (46). Genera confirmed by Boruta analysis were considered high-confidence biomarkers, and model performance was evaluated using OOB error and cross-validation. The combined results from these algorithms were used to shortlist microbial taxa with strong discriminatory power across treatments.

Results

Effects of garlic oil and rubber seed oil on rumen fermentation and methane production

Dry matter digestibility and gas production

GO markedly reduced DMD and total gas production relative to the CON and RO treatments ($p < 0.001$) (Table 2). Specifically, the DMD declined from 70.7% in the CON to 64.1–66.8% in the GO treatments, whereas total gas production decreased from 127.4–131.3 mL to 112.2–115.1 mL. However, RO alone did not significantly affect these parameters.

The cumulative gas production profiles observed over a 24 h incubation period consistently showed lower rates in the GO treatments (Fig. 1a and Fig. 1b). To clarify the temporal dynamics, Table 2 details how treatments influence cumulative *in vitro* gas production at 3, 6, 12, and 24 h. No significant differences among treatments were found at 3 h ($P = 0.700$), with gas production ranging from 32.7 to 34.7 mL. From 6 h onward, significant effects appeared ($P < 0.001$). At 6 h, the CON and RO groups produced higher gas volumes (22.7–23.5 mL) compared to GO and GORO groups (19.6–20.4 mL), with GO, GORO2, and GORO showing lower values. These patterns continued at 12 h (CON/RO: 29.8–31.6 mL vs. GO/GORO: 24.5–25.1 mL) and 24 h (CON/RO: 35.9–36.7 mL vs. GO/GORO: 30.6–31.4 mL), with GO-containing treatments consistently producing less gas ($P < 0.05$). The time-course profiles (Fig. 1b) illustrate that GO and combined GORO treatments resulted in lower cumulative gas accumulation over the 24 h incubation period, while RO supplementation alone mirrored CON levels, confirming its limited independent impact on fermentation kinetics.

Volatile fatty acid profiles

Total VFA concentrations remained unchanged across treatments (p = 0.08); however, individual VFA proportions exhibited significant shifts with the application of GO (Table 2). Specifically, acetate proportions decreased from 62.1–62.7 to 58.4–58.8mol/100 mol, whereas propionate (19.6–19.9 to 21.2–21.6 mol/100 mol) and butyrate (13.3–13.8 to 15.4–15.9 mol/100 mol) increased (p < 0.001). Consequently, the acetate to propionate ratios were reduced from 3.12–3.19 to 2.72–2.77.

Methane production, Ammonia Nitrogen (NH_3-N), and microbial counts

GO consistently reduced methane production by approximately 50% across all treatments (6.82 mL in the CON vs. 3.21–3.66 mL in GO; p < 0.001) (Table 2). Methane per gram of digested dry matter also decreased from 19.3 to 9.73–11.1 mL/g. Total protozoa counts were significantly lower in the GORO treatments (5.45 vs. 5.22–5.26 $\log_{10}$; p < 0.001). However, the RO-alone treatment group did not show methane-reducing effects. Ammonia nitrogen (NH_3-N) concentrations also varied significantly among treatments (p < 0.001; Table 1). The CON group averaged 22.0 mg/dL, while GORO4 (24.79 mg/dL) and GORO (24.1 mg/dL) exhibited numerically higher NH_3-N levels. In contrast, GO treatment (22.2 mg/dL) remained comparable to CON.

Multivariate analysis

The treatments were clearly separated in the PCA of fermentation traits, with PC1 capturing the primary variance between the GO and CON/RO groups (Fig. 1c). Methane production parameters showed the highest positive loadings on PC1 (0.97–0.98), which correlated strongly with acetate proportion and A:P ratio, while propionate and butyrate showed negative loadings (0.87 to 0.95) (Fig. 1d and Table S1). Spearman's correlation analysis revealed that methane parameters presented strong positive correlations with the acetate proportion (ρ = 0.81, p < 0.001) and A:P ratio (ρ = 0.84, p < 0.001) and negative correlations with propionate (ρ = –0.75) and butyrate (ρ = –0.78) (Fig. 1e).

Microbial community analysis

Microbial community analyses via 16S rRNA sequencing were conducted on selected treatments (CON, GO, and the high-dose GORO) to focus on key effects, including elevated NH_3-N in GORO.

Alpha and beta diversity

The GO treatment significantly reduced across all alpha diversity indices relative to the CON and GORO treatments: Chao1 (865 vs. 1257 CON; $p = 0.008$), Shannon diversity (7.82 vs. 9.31; $p = 0.002$), and evenness (0.802 vs. 0.905; $p = 0.002$) (Table 3, Fig. 2a). The GORO treatment partially restored the diversity levels. Beta diversity analysis revealed distinct community structures among the treatments ($R^2 = 0.93$, $p = 0.001$) (Fig. 2b).

Microbial abundance changes

Analysis of the UpSet diagram revealed complex patterns of taxonomic overlap and exclusivity among treatments (Fig. 3a–c). At the phylum level, communities showed broad convergence, sharing 18 phyla across all treatments (CON, GO, GORO). However, clear treatment-specific signatures were present, with 4, 2, and 3 phyla uniquely linked to CON, GO, and GORO, respectively. Family-level analysis provided more detail, with 127 families shared among treatments, and 23, 8, and 19 families uniquely enriched in CON, GO, and GORO, respectively. At the genus level, divergence was most evident: although 198 genera were common to all treatments, 45, 12, and 38 genera were exclusive to CON, GO, and GORO, respectively. These hierarchical patterns emphasize the step-by-step development of treatment-specific microbial signatures, with more detailed taxonomic levels uncovering clearer community structure distinctions.

Notably, the relative abundance profiles of the top 25 phyla, families, and genera displayed marked heterogeneity among treatments (Fig. 3d–f), highlighting shifts in dominant lineages that may underpin functional variation across microbial assemblages.

At the phylum level, GO administration resulted in a significant increase in Bacillota (61.3% compared to 50.4% in CON, decreased Bacteroidota (34.4% compared to 43.3%), and nearly eradicated Spirochaetota (0.4% compared to 2.8%) ($p < 0.05$) (Table S2). Furthermore, Methanobacteriota was markedly diminished in both GO and GORO treatment groups (0.1%

compared to 0.66% in CON). Notably, the GORO treatment increased Actinomycota (*p*-adjusted = 0.012) and Fibrobacterota (*p*-adjusted = 0.012).

At the family level, a clear restructuring of microbial communities was observed (Table S3). Among the twenty-five most abundant families, several experienced significant shifts in their relative abundance. Notably, *Selenomonadaceae* increased markedly in the GO group (31.3%) compared to the control (1.16%) and GORO (3.0%) groups (*p*-adjusted = 0.030), indicating strong selective growth. Conversely, *Prevotellaceae* declined substantially under GO treatment (11.8%) relative to the control (20.0%) and GORO (16.8%) groups (*p*-adjusted = 0.030), reflecting suppression of this group. *Oscillospiraceae* showed two responses: a significant decrease in GO (7.3%) but an increase in GORO (15.8%) compared to the control (12.2%) (*p*-adjusted = 0.030). These findings illustrate how different treatments influence key microbial families, with GO exerting strong selective pressure and GORO aiding in community restoration.

At the genus level, GO administration led to notable changes, including significant increases in *Selenomonas* (from 1.9% in the CON to 10.7% in GO) and *Roseburia* (from 2.0% to 11.0%). Conversely, *Methanobrevibacter* exhibited a considerable decrease in relative abundance in the GO (0.55%) and GORO (0.26%) treatments compared to the CON group (2.3%) (*p*-value = 0.012) (Table S4 and Fig. 4a). The GORO treatment exhibited distinct microbial patterns, marked by increased levels of *Ruminococcus* (8.2%) and *Fibrobacter* (1.9%).

Differential abundance and biomarker analysis

Volcano plot analyses identified extensive shifts in genus-level abundance across treatment comparisons (Fig. 3g–i). The GO versus CON contrast exhibited the most pronounced alterations, with multiple genera significantly enriched or depleted, reflecting substantial community restructuring. In comparison, the GORO versus CON analysis revealed more moderate changes, suggesting partial modulation of microbial composition (Table S6). Strikingly, the GORO versus GO comparison highlighted a restorative effect of the combination treatment, attenuating extreme abundance shifts and indicating a potential rebalancing of microbial community structure.

The DESeq2 analysis identified 21 significantly different genera between GO and CON treatments, with notable enrichments in *Propionispira* (+23.9 log_2FC), *Anaerovibrio* (+23.3), and *Megasphaera* (+12.9) (Fig. 3g&i; Tables S5&S7). The Random Forest classification achieved 100% accuracy (Table S8) and identified *Selenomonas* as the most predictive biomarker (Mean Decrease Accuracy: 7.18) (Fig. 4b, Table S9). Boruta feature selection identified 25 genera as robust biomarkers that discriminated the GO treatment from the CON treatment. Thus, these genera are potential indicators of enhanced propionate fermentation and reduced methanogenic activity (Fig. 4c–d).

Correlation network analysis

Clostridium was strongly positively correlated with methane production parameters ($\rho = 0.85$, $p < 0.0001$), the acetate proportions ($\rho = 0.86$), and A:P ratios ($\rho = 0.91$). Conversely, *Parabacteroides* was negatively correlated with methane production ($\rho = 0.71$, $p = 0.003$), suggesting its potential role in mitigating methane (Fig. 4e, Table S10). Network analysis identified five keystone genera with high betweenness centrality, suggesting their critical roles in fermentation processes (Fig. 4f).

Functional profiling

Enzyme Commission (EC) profile analysis revealed significant functional shifts with treatments ($R^2 = 0.95$, $p = 0.001$) (Fig. 5a). A heatmap of the top 25 most variable EC numbers demonstrated distinct clustering patterns, with the GO treatments exhibiting elevated expression in enzymatic classes EC:3.1.21.3, EC:1.6.5.3, EC:1.97.1.4, and EC:2.7.1.11 (Fig. 5b and Fig. 5c. and Table S12). The GO treatment altered multiple enzymatic pathways, notably upregulating EC:3.5.1.101 (+7.15 log_2FC) and EC:5.3.1.26 (+6.61 log_2FC), while downregulating EC:3.6.1.25 (–7.16 log_2FC) and EC:3.2.1.97 (–9.47 log_2FC) (Fig. 5d, Table S13). The GORO treatment elicited more targeted enzymatic responses (Fig. 5e, Table S14), with a direct comparison to GO alone indicating synergistic interactions (Fig. 5f, Table S15).

Discussion

This study demonstrates that GO and GORO treatments significantly reduced methane emissions by approximately 50% and altered rumen fermentation patterns. The GO treatment enhanced propionate and butyrate production at the expense of acetate, indicating a metabolic shift from methanogenesis to more energy-efficient pathways. However, these advantages were counterbalanced by reductions in DMD (6.2–9.3%) and total gas production (12.1–14.6%), suggesting antimicrobial effects on fiber-degrading bacteria.

Mechanisms of methane reduction

The observed decrease in methane levels was directly correlated with the reduction in *Methanobrevibacter* relative abundance (76% decrease in the GO treatment), thereby confirming that this genus is the primary target for methanogenic activity. Organosulfur compounds present in GO, especially allicin, are likely to inhibit methyl-coenzyme M reductase via thiol-reactive mechanisms, thereby disrupting the final step of methanogenesis (47, 48). This specific inhibition elucidates why bacterial populations remained largely unaffected, while methanogenic archaea were suppressed.

Compared to the CON treatment, the metabolic shift towards increased propionate production in the GO treatment (8.2-10.2%) indicates a reallocation of hydrogen via the succinate pathway, which is supported by the proliferation of propionate-producing genera such as *Selenomonas* (5.6–fold increase) and upregulation of methylmalonyl-CoA decarboxylase (EC:4.1.1.85, +6.60 $\log_2$FC). Significant correlations between the abundance of *Selenomonas* and propionate levels ($\rho = 0.88$, $p < 0.0001$) substantiate the functional role of this genus in this metabolic redirection (49, 50). Similarly, the enrichment of *Roseburia* (5.5-fold) contributed to elevated butyrate production through the acetyl-CoA pathway (51). GO-containing treatments reduced methane production by ~50%, and a ~2 percentage point increase in propionate proportion (Table 2) aligns with the targeted suppression of methanogens and the concurrent enrichment of hydrogen-utilizing bacteria, such as *Selenomonas* and *Roseburia*, as revealed by 16S rRNA gene sequencing. In contrast, RO alone did not significantly alter methane or VFA profiles, consistent with its limited direct impact on methanogens but evident

role in modulating overall community resilience. For instance, the numerically higher NH_3-N levels in GORO treatments (e.g., 24.79 mg/dL in GORO4 vs. 22.0 mg/dL in CON; Table 1) may reflect enhanced protein degradation facilitated by preserved microbial diversity and enriched proteolytic taxa, without compromising total gas production or digestibility. This integration underscores RO's protective contribution: by mitigating GO-induced disruptions to non-target microbes (e.g., maintaining protozoa counts closer to CON levels in GORO; Table 2), RO supports a balanced fermentation environment that sustains methane mitigation while preventing adverse shifts in metabolite outputs, as further evidenced by predicted pathway analyses showing restored fiber-degrading enzymes in combined treatments.

Rubber seed oil's protective effects

A key finding of this study is the capacity of RO to mitigate the adverse effects of GO on microbial diversity and fiber degradation, while concurrently maintaining methane reduction. The GORO treatment preserved microbial richness comparable to that under the CON conditions (Chao1: 1,256 vs. 1,257) and enriched cellulolytic taxa such as *Ruminococcus* (8.2% vs. 2.16% in CON) and *Fibrobacter* (1.9% vs. 0.45%) (52). This protective effect was likely caused by multiple mechanisms: (1) membrane stabilization through nonpolar compounds to reduce GO accessibility, (2) alternative carbon source provision to enhance metabolic flexibility, and (3) biofilm formation to create a protective barrier against antimicrobial stress (53, 54). The enzymatic analysis corroborated this protective role, with the GORO treatment partially restoring endo-1,4-β-xylanase activity (EC:3.2.1.97) while upregulating butyrate-CoA ligase (EC:2.8.3.21, +4.74 log_2FC), indicating improved fiber degradation and energy metabolism. Furthermore, the 6.4% increase in Actinomycetota, especially *Eggerthellaceae*, demonstrated an enhanced capacity for lignocellulosic degradation under the GORO treatment (55).

Network analysis and biomarker identification

Network analysis revealed that *Clostridium* acted as a keystone genus based on its highest connectivity (Table S11) and strong positive correlations with methane production ($\rho = 0.85$, $p < 0.0001$) and acetate levels ($\rho = 0.86$). This observation corroborates its role in the production of hydrogen and formate during carbohydrate fermentation, which serve as substrates for methanogenic archaea (56). Conversely, *Parabacteroides* demonstrated a negative correlation with methane ($\rho = 0.71$, $p = 0.003$), thereby serving as a biomarker of low-methane systems through its dual pathways for acetate and propionate production (57). Machine learning classification achieved perfect accuracy (100%) in differentiating treatments, with *Selenomonas* identified as the most predictive biomarker (Mean Decrease Accuracy: 7.18, $p = 0.010$). This robust classification underscores the potential for microbial biomarker-based monitoring of methane mitigation strategies. The Boruta feature selection process identified 25 robust biomarkers, including *Porphyromonas* and *Sporomusa*, which exhibited strong negative correlations with methane emissions via hydrogen diversion mechanisms (58).

Mechanistic insights into enzymatic reprogramming induced by GO and GORO supplementation

Supplementation with GO initiated a coordinated cascade of enzymatic responses, thus representing the mechanistic underlying the approximately 50% reduction in methane emissions observed within the rumen. The most notable upregulation was identified for EC:4.1.1.85 (methylmalonyl-CoA decarboxylase; $\log_2FC = +6.60$), a diagnostic enzyme within the succinate pathway of propionate synthesis. This enzyme facilitates the decarboxylation of methylmalonyl-CoA to propionyl-CoA, a pivotal step in redirecting hydrogen from methanogenesis to propionogenesis (59). Its activity was correlated with several genera responsible for propionate production, including *Dialister, Roseburia, Prevotella, and Sodaliphilus* (60, 61). The increased expression of EC:4.1.1.85 was correlated with the higher molar proportion of propionate observed under GO treatment (21.2–21.6 vs. 19.6–19.9 mol/100 mol), thereby supporting a strategic alteration in hydrogen utilization that restricts substrate

availability for methanogenic archaea (11, 62, 63). Moreover, the upregulation of cellulose synthase (EC:2.4.1.5; log_2FC = +6.60) indicated a microbial compensatory response to GO's antimicrobial stress. Increased cellulose production is a well-documented adaptation to environmental stressors that helps strengthen the cell wall and support microbial survival (64-66). This likely explains the observed decrease in DMD, despite the constant total VFA output, thus revealing a trade–off between microbial resilience and feed utilization efficiency.

In contrast, the GO treatment inhibited key fibrolytic and nitrogen-related enzymes. EC:3.2.1.97 (endo-1,4-β-xylanase; log_2FC= –9.47), which is important for hemicellulose breakdown, was significantly downregulated by GO, corresponding to a 6.2–9.3% reduction in DMD. This reduction in fiber digestion indicates a shift toward less efficient digestive processes. Additionally, EC:5.4.99.23 (chorismate mutase; log_2FC = –4.71), a critical enzyme in the shikimate pathway, was suppressed by GO, thus indicating changes in aromatic amino acid production and nitrogen metabolism (67, 68).

Beyond abundance shifts, GO caused a fundamental restructuring of microbial metabolic functions. Upregulation of aminoacylase (EC:3.5.1.101) indicates enhanced amino acid recycling, a known adaptive strategy for nitrogen conservation under antimicrobial stress (69, 70). This functional shift is consistent with the observed differences in NH_3–N concentrations, as increased amino acid recycling reduces deamination and free ammonia release (71). Such nitrogen conservation strategies highlight microbial adaptation to maintain growth and microbial balance under antimicrobial pressure, linking enzymatic activity with measurable changes in nitrogen turnover. Modulation of pentose phosphate pathway enzymes, especially ribose-5-phosphate isomerase (EC:5.3.1.26), indicated increased NADPH demand for redox balancing in response to oxidative stress from garlic-derived organosulfur compounds (72). The induction of glutamate–cysteine ligase (EC:6.3.2.7), the rate-limiting enzyme in glutathione biosynthesis, further supported the activation of thiol-based antioxidant defenses (73, 74).

GORO treatment: functional compensation and metabolic refinement

GORO triggered a more detailed enzymatic response and partially reduced the adverse effects of GO. The upregulation of EC:2.8.3.21 (butyrate-CoA ligase; $log_2FC = +4.74$) and EC:1.8.5.3 (ferredoxin-NADP reductase; $log_2FC = +4.73$) indicates improved butyrate metabolism and energy production. Butyrate-CoA ligase activates butyrate for βoxidation, which explains the higher butyrate levels (15.4–15.9 vs. 13.3–13.8 mol/100 mol) without corresponding increases in total VFAs (71, 75).

A direct comparison between GO and GORO revealed a significant downregulation of EC:4.1.1.85 ($log_2FC = –7.96$) in the GORO treatment, indicating a decreased reliance on the succinate pathway. This observation may suggest a metabolic shift toward alternative propionate-producing routes, such as the acrylate or lactate pathways, which are less disruptive to microbial ecology (76, 77). Furthermore, the downregulation of methylmalonyl-CoA decarboxylase could result in the accumulation of (S)-methylmalonyl-CoA, which may be diverted into branched-chain fatty acid synthesis (78-80).

Conversely, EC:3.2.1.97 (endo-1,4-β-xylanase) was significantly upregulated in GORO ($log_2FC = +7.09$), indicating a partial recovery of fiber degradation capacity (81). Additional upregulation of carnitine acetyltransferase (EC:2.8.3.21) suggested improved fatty acid oxidation and acetyl-CoA turnover, and thus improved energy efficiency (82, 83). Restoration of nucleotide metabolism, as evidenced by increased phosphohydrolase (EC:3.6.1.25) activity, further supports microbial stability and metabolic resilience (84).

These enzymatic shifts collectively demonstrate a dual mechanism of methane mitigation: (1) direct inhibition of methanogens through allicin's thiol-reactive properties (10, 85), and (2) redirection of hydrogen flux via enzymatic reprogramming of bacterial metabolism. The specificity of these pathway-targeted modifications, rather than generalized metabolic suppression, exemplifies the complexity of microbial adaptations to phytogenic interventions.

Overall, GO induced oxidative and metabolic stress, triggering antioxidant defenses and redirecting metabolism, whereas RO mitigated these effects, promoting energy-efficient and environmentally stable microbial states. Therefore, the GORO treatment offered a balanced approach that maintains fiber degradability and microbial diversity while reducing methane emissions. These findings provide a mechanistic framework for designing targeted dietary strategies to optimize rumen function and mitigate methane's environmental impact.

Implications, limitations, and future directions

The findings show that targeted microbial manipulation through synergistic phytogenic combinations can reduce methane emissions without affecting rumen function. The GORO treatment offers a balanced method that redirects hydrogen away from methanogenesis while maintaining important fiber breakdown and energy processes. The microbial biomarkers identified here may serve as tools for real-time monitoring and improving methane reduction strategies. Future research should focus on testing these mechanisms in live animals and optimizing doses to maximize benefits and minimize any negative impacts on animal performance. The biomarker framework developed here has potential for personalized rumen management that is tailored to individual animal microbiomes (86).

While this *in vitro* study provides valuable insights into the combined effects of GO and RO on rumen methane mitigation, several limitations should be noted. A key constraint is that microbial sequencing was limited to CON, GO, and the high-dose combination GORO treatment, rather than all individual RO doses, due to resource limitations. This approach prioritized investigating specific outcomes, such as the elevated NH_3-N in GORO, but may obscure potential dose-dependent microbial shifts across lower RO levels. However, analyses of other fermentation parameters (e.g., methane production, VFAs, gas kinetics) across all treatments support the study's conclusions on RO's protective role. Future research should employ comprehensive metagenomic sequencing in

dose-response designs, ideally *in vivo*, to refine optimal supplementation levels, explore long-term impacts on animal performance, and further elucidate mechanisms underlying NH_3-N variations.

Conclusion

This study offers mechanistic insights into the methane-reducing effects of GO and demonstrates the protective role of RO in maintaining rumen function. The combination treatment facilitates targeted metabolic reprogramming through selective microbial enrichment and enzymatic modulation, thereby providing a sustainable approach to reducing greenhouse gas emissions from livestock while preserving rumen health and productivity. The identified biomarkers enable precise monitoring of these interventions, thereby advancing the development of more effective and environmentally sustainable strategies for ruminant nutrition. The findings of this study will enable more precise monitoring of EO interventions and advance the development of more effective and environmentally sustainable strategies for ruminant nutrition.

Competing Interests

Authors Gihwal Son and Jaeyong Song were employed by the Nonghyup Livestock Research Center and Nonghyup Feed Co., Ltd., respectively. The remaining authors declare that the research was conducted in the absence of any commercial or financial relationships that could be construed as a potential conflict of interest.

Funding sources

This research was supported by the Hanwoo research project (2024) of the Nonghyup Feed Co., Ltd.

Data availability statement

The datasets generated in this study are available in online repositories. The repository name(s) and corresponding accession number(s) can be accessed in the NCBI database: https://www.ncbi.nlm.nih.gov/bioproject/PRJNA1377940.

Acknowledgments

This research was also supported by the Chung–Ang University Graduate Research Scholarship (Academic scholarship for the College of Biotechnology and Natural Resources) in 2025.

References

1. Johnson KA, Johnson DE. Methane emissions from cattle. Journal of animal science. 1995;73(8):2483-92.
2. Cuervo W, Gomez-Lopez C, & , DiLorenzo N. Methane Synthesis as a Source of Energy Loss Impacting Microbial Protein Synthesis in Beef Cattle—A Review. Methane. 2025;4(2):10.
3. Tseten T, Sanjorjo RA, Kwon M, Kim SW. Strategies to Mitigate Enteric Methane Emissions from Ruminant Animals. J Microbiol Biotechnol. 2022;32(3):269-77.
4. Wedlock DN, Janssen PH, Leahy SC, Shu D, Buddle BM. Progress in the development of vaccines against rumen methanogens. Animal. 2013;7 Suppl 2:244-52.
5. Knapp JR, Laur GL, Vadas PA, Weiss WP, Tricarico JM. Invited review: Enteric methane in dairy cattle production: quantifying the opportunities and impact of reducing emissions. Journal of dairy science. 2014;97(6):3231-61.
6. Patra A, Park T, Kim M, Yu Z. Rumen methanogens and mitigation of methane emission by anti-methanogenic compounds and substances. Journal of animal science and biotechnology. 2017;8:13.
7. Belanche A, Newbold CJ, Morgavi DP, Bach A, Zweifel B, Yanez-Ruiz DR. A Meta-analysis Describing the Effects of the Essential oils Blend Agolin Ruminant on Performance, Rumen Fermentation and Methane Emissions in Dairy Cows. Animals (Basel). 2020;10(4).
8. Wells CW. Effects of essential oils on economically important characteristics of ruminant species: A comprehensive review. Animal nutrition. 2024;16:1-10.
9. Sari NF, Ray P, Rymer C, Kliem KE, Stergiadis S. Garlic and Its Bioactive Compounds: Implications for Methane Emissions and Ruminant Nutrition. Animals (Basel). 2022;12(21):2998.
10. M. Busquet SC, A. Ferret, P. W. Cardozo, and C. Kamel. Effects of Cinnamaldehyde and Garlic Oil on Rumen Microbial Fermentation in a Dual Flow Continuous Culture. J Dairy Sci. 2005; 88:2508–16.
11. Martin RSH, Chaudhry AS. The effects of garlic as a feed additive on ruminal fermentability and ruminant performance: A meta-analysis. Journal of agriculture and food research. 2024;18:101531.
12. Gunun P, Laorodphan N, Phayom W, Kaewwongsa W, Kaewpila C, Khota W, et al. Effects of supplementing rumen-protected rubber seed oil to dairy cattle on feed digestibility and milk production. Animal bioscience. 2025;38(4):665-72.
13. Pi Y, Ma L, Pierce KM, Wang HR, Xu JC, Bu DP. Rubber seed oil and flaxseed oil supplementation alter digestion, ruminal fermentation and rumen fatty acid profile of dairy cows. Animal. 2019;13(12):2811-20.
14. Tseten T, Sanjorjo RA, Kwon M, Kim SW. Strategies to Mitigate Enteric Methane Emissions from Ruminant Animals. J Microbiol Biotechnol. 2022;32(3):269-77.
15. Sun X, Wang Y, Ma X, Li S, Wang W. Producing natural functional and low-carbon milk by regulating the diet of the cattle—The fatty acid associated rumen fermentation, biohydrogenation, and microorganism response. Frontiers in Nutrition. 2022;Volume 9 - 2022.
16. Pi Y, Gao ST, Ma L, Zhu YX, Wang JQ, Zhang JM, et al. Effectiveness of rubber seed oil and flaxseed oil to enhance the α-linolenic acid content in milk from dairy cows. Journal of Dairy Science. 2016;99(7):5719-30.
17. Cardozo P, Calsamiglia S, Ferret A, Kamel C. Effects of natural plant extracts on ruminal protein degradation and fermentation profiles in continuous culture. Journal of animal science. 2004;82(11):3230-6.
18. Patra AK, Yu Z. Effects of Essential Oils on Methane Production and Fermentation by, and Abundance and Diversity of, Rumen Microbial Populations. Applied and Environmental Microbiology. 2012;78(12):4271-80.

19. Amanullah SM, Lee S-S, Paradhipta DHV, Joo Y-H, Kim D-H, Seong P-N, et al. Impact of Oil Sources on In Vitro Fermentation, Microbes, Greenhouse Gas, and Fatty Acid Profile in the Rumen. Fermentation. 2022;8(5):242.
20. Kliem KE, Humphries DJ, Kirton P, Givens DI, Reynolds CK. Differential effects of oilseed supplements on methane production and milk fatty acid concentrations in dairy cows. animal. 2019;13(2):309-17.
21. Patra AK. The effect of dietary fats on methane emissions, and its other effects on digestibility, rumen fermentation and lactation performance in cattle: A meta-analysis. Livestock Science. 2013;155(2):244-54.
22. Goering HK, Van Soest PJ. Forage fiber analyses (apparatus, reagents, procedures, and some applications): US Agricultural Research Service; 1970.
23. Thauer RK, Kaster AK, Seedorf H, Buckel W, &, Hedderich R. A simple gas production method using a pressure transducer to determine the fermentation kinetics of ruminant feeds. Animal feed science and technology. 1994;48(3-4):185-97.
24. Ceron-Chafla P, García-Timermans C, De Vrieze J, Ganigué R, Boon N, Rabaey K, et al. Pre-incubation conditions determine the fermentation pattern and microbial community structure in fermenters at mild hydrostatic pressure. Biotechnology and Bioengineering. 2022;119(7):1792-807.
25. Chaney AL, Marbach EP. Modified reagents for determination of urea and ammonia. Clinical chemistry. 1962;8(2):130-2.
26. Hamid MMA, Moon J, Yoo D, Kim H, Lee YK, Song J, et al. Rumen fermentation, methane production, and microbial composition following in vitro evaluation of red ginseng byproduct as a protein source. Journal of animal science and technology. 2020;62(6):801-11.
27. Yu Z, Morrison M. Improved extraction of PCR-quality community DNA from digesta and fecal samples. Biotechniques. 2004;36(5):808-12.
28. Nadkarni MA, Martin FE, Jacques NA, Hunter N. Determination of bacterial load by real-time PCR using a broad-range (universal) probe and primers set. Microbiology. 2002;148(1):257-66.
29. Bolyen E, Rideout JR, Dillon MR, Bokulich NA, Abnet CC, Al-Ghalith GA, et al. Reproducible, interactive, scalable and extensible microbiome data science using QIIME 2. Nature biotechnology. 2019;37(8):852-7.
30. Martin M. Cutadapt removes adapter sequences from high-throughput sequencing reads. EMBnet journal. 2011;17(1):10-2.
31. Callahan BJ, Wong J, Heiner C, Oh S, Theriot CM, Gulati AS, et al. High-throughput amplicon sequencing of the full-length 16S rRNA gene with single-nucleotide resolution. Nucleic acids research. 2019;47(18):e103.
32. Quast C, Pruesse E, Yilmaz P, Gerken J, Schweer T, Yarza P, et al. The SILVA ribosomal RNA gene database project: improved data processing and web-based tools. Nucleic acids research. 2013;41(Database issue):D590-6.
33. Kaehler BD, Bokulich NA, McDonald D, Knight R, Caporaso JG, Huttley GA. Species abundance information improves sequence taxonomy classification accuracy. Nature communications. 2019;10(1):4643.
34. Bokulich NA, Kaehler BD, Rideout JR, Dillon M, Bolyen E, Knight R, et al. Optimizing taxonomic classification of marker-gene amplicon sequences with QIIME 2's q2-feature-classifier plugin. Microbiome. 2018;6(1):90.
35. Oksanen J, Simpson G, Blanchet F, Roeland K, Legendre P, Minchin P, et al. vegan (v2. 6-4). R. 2022.
36. Douglas GM, Maffei VJ, Zaneveld JR, Yurgel SN, Brown JR, Taylor CM, et al. PICRUSt2 for prediction of metagenome functions. Nature biotechnology. 2020;38(6):685-8.
37. McMurdie PJ, Holmes S. phyloseq: an R package for reproducible interactive analysis and graphics of microbiome census data. PloS one. 2013;8(4):e61217.

38. Wickham H. Data analysis. ggplot2: elegant graphics for data analysis: Springer; 2016. p. 189-201.
39. Kolde R. pheatmap: Pretty Heatmaps. R package version 1.0. 13 (2025-06-05). Vienna, Austria: R Foundation for Statistical Computing.[WWW document] URL …; 2025.
40. Love MI, Huber W, Anders S. Moderated estimation of fold change and dispersion for RNA-seq data with DESeq2. Genome biology. 2014;15(12):550.
41. Kassambara A, Mundt F. Package 'factoextra'. Extract and visualize the results of multivariate data analyses. 2017;76(2):10.18637.
42. Csardi G, & Csardi, M. G. . The igraph package. Citeseer; 2007.
43. Pedersen TL, Pedersen M, LazyData T, Rcpp I, Rcpp L. Package 'ggraph'. Retrieved January. 2017;1:2018.
44. RColorBrewer S, Liaw MA. Package 'randomforest'. University of California, Berkeley: Berkeley, CA, USA. 2018.
45. Archer E, Archer ME. Package 'rfPermute'. R Project: Indianapolis, IN, USA. 2016.
46. Kursa MB, Rudnicki WR. Feature Selection with the Boruta Package. Journal of statistical software. 2010;36(11):1-13.
47. Borlinghaus J, Albrecht F, Gruhlke MC, Nwachukwu ID, Slusarenko AJ. Allicin: chemistry and biological properties. Molecules. 2014;19(8):12591-618.
48. Thauer RK. Methyl (Alkyl)-Coenzyme M Reductases: Nickel F-430-Containing Enzymes Involved in Anaerobic Methane Formation and in Anaerobic Oxidation of Methane or of Short Chain Alkanes. Biochemistry. 2019;58(52):5198-220.
49. Scheifinger CC, Wolin MJ. Propionate formation from cellulose and soluble sugars by combined cultures of Bacteroides succinogenes and Selenomonas ruminantium. Applied microbiology. 1973;26(5):789-95.
50. Jeong J, Yu C, Kang R, Kim M, Park T. Application of propionate-producing bacterial consortium in ruminal methanogenesis inhibited environment with bromoethanesulfonate as a methanogen direct inhibitor. Frontiers in veterinary science. 2024;11:1422474.
51. Duncan SH, Barcenilla A, Stewart CS, Pryde SE, Flint HJ. Acetate utilization and butyryl coenzyme A (CoA):acetate-CoA transferase in butyrate-producing bacteria from the human large intestine. Applied and environmental microbiology. 2002;68(10):5186-90.
52. Koike S, Kobayashi Y. Fibrolytic Rumen Bacteria: Their Ecology and Functions. Asian-Australasian Journal of Animal Sciences. 2009;22(1):131-8.
53. Zhou J, Richlen ML, Sehein TR, Kulis DM, Anderson DM, Cai Z. Microbial Community Structure and Associations During a Marine Dinoflagellate Bloom. Frontiers in microbiology. 2018;9:1201.
54. Flemming HC, Wingender J. The biofilm matrix. Nature reviews microbiology. 2010;8(9):623-33.
55. Saini A, Aggarwal NK, Sharma A, Yadav A. Actinomycetes: A Source of Lignocellulolytic Enzymes. Enzyme research. 2015;2015(1):279381.
56. Janssen PH. Influence of hydrogen on rumen methane formation and fermentation balances through microbial growth kinetics and fermentation thermodynamics. Animal feed science and technology. 2010;160(1-2):1-22.
57. Reichardt N, Duncan SH, Young P, Belenguer A, McWilliam Leitch C, Scott KP, et al. Phylogenetic distribution of three pathways for propionate production within the human gut microbiota. The ISME journal 2014;8(6):1323-35.
58. Krause DO, Denman SE, Mackie RI, Morrison M, Rae AL, Attwood GT, et al. Opportunities to improve fiber degradation in the rumen: microbiology, ecology, and genomics. FEMS microbiology reviews. 2003;27(5):663-93.
59. Zhou Y, Gao YH, Zhang BC, Yang HL, Tian YB, Huang YH, et al. CELLULOSE SYNTHASE-LIKE C proteins modulate cell wall establishment during ethylene-mediated root growth inhibition in rice. Plant Cell. 2024;36(9):3751-69.

60. Rivera I, Harlow K, Cole RN, O'Meally R, Garrett W, Xiong W, et al. A metaproteomic analysis of the piglet fecal microbiome across the weaning transition. Frontiers in microbiology. 2025;16:1504433.
61. Gharechahi J, Sarikhan S, Han JL, Ding XZ, Salekdeh GH. Functional and phylogenetic analyses of camel rumen microbiota associated with different lignocellulosic substrates. NPJ biofilms microbiomes. 2022;8(1):46.
62. Ding H, Ao C, Zhang X. Potential use of garlic products in ruminant feeding: A review. Animal nutrition. 2023;14:343-55.
63. Patra AK, Yu Z. Effects of Adaptation of In vitro Rumen Culture to Garlic Oil, Nitrate, and Saponin and Their Combinations on Methanogenesis, Fermentation, and Abundances and Diversity of Microbial Populations. Front Microbiol. 2015;6:1434.
64. Ntatsi G, Savvas D, Papasotiropoulos V, Katsileros A, Zrenner RM, Hincha DK, et al. Rootstock Sub-Optimal Temperature Tolerance Determines Transcriptomic Responses after Long-Term Root Cooling in Rootstocks and Scions of Grafted Tomato Plants. Frontiers in plant science. 2017;8:911.
65. Singh S, Sharma R, Nepolean T, Nayak SN, Pushpavathi B, Khan AW, et al. Identification of genes controlling compatible and incompatible reactions of pearl millet (Pennisetum glaucum) against blast (Magnaporthe grisea) pathogen through RNA-Seq. Frontiers in plant science. 2022;13:981295.
66. Kesten C, Menna A, Sanchez-Rodriguez C. Regulation of cellulose synthesis in response to stress. Current opinion in plant biology. 2017;40:106-13.
67. Nazmi AR, Lang EJM, Bai Y, Allison TM, Othman MH, Panjikar S, et al. Interdomain Conformational Changes Provide Allosteric Regulation en Route to Chorismate. Journal of Biological Chemistry. 2016;291(42):21836-47.
68. Jiao W, Fan Y, Blackmore NJ, Parker EJ. A single amino acid substitution uncouples catalysis and allostery in an essential biosynthetic enzyme in Mycobacterium tuberculosis. Journal of Biological Chemistry. 2020;295(19):6252-62.
69. Youshko MI, van Langen LM, Sheldon RA, Švedas VK. Application of aminoacylase I to the enantioselective resolution of α-amino acid esters and amides. Tetrahedron: Asymmetry. 2004;15(12):1933-6.
70. Min L, Zhao S, Tian H, Zhou X, Zhang Y, Li S, et al. Metabolic responses and "omics" technologies for elucidating the effects of heat stress in dairy cows. International journal of biometeorology. 2017;61(6):1149-58.
71. Russell J, Wallace R. Energy-yielding and energy-consuming reactions. In The rumen microbial ecosystem,. Dordrecht: Springer Netherlands1997. p. 246-82.
72. Stincone A, Prigione A, Cramer T, Wamelink MM, Campbell K, Cheung E, et al. The return of metabolism: biochemistry and physiology of the pentose phosphate pathway. Biological reviews. 2015;90(3):927-63.
73. Griffith OW. Biologic and pharmacologic regulation of mammalian glutathione synthesis. Free radical biology and medicine. 1999;27(9-10):922-35.
74. Georgiou-Siafis SK, Tsiftsoglou AS. The Key Role of GSH in Keeping the Redox Balance in Mammalian Cells: Mechanisms and Significance of GSH in Detoxification via Formation of Conjugates. Antioxidants (Basel). 2023;12(11):1953.
75. Flint HJ, Scott KP, Duncan SH, Louis P, Forano E. Microbial degradation of complex carbohydrates in the gut. Gut microbes. 2012;3(4):289-306.
76. Gottschalk G. Bacterial fermentations. Bacterial metabolism: Springer; 1986. p. 208-82.
77. Diekert G, Wohlfarth G. Metabolism of homocetogens. Antonie Van Leeuwenhoek. 1994;66(1-3):209-21.
78. Dewulf JP, Gerin I, Rider MH, Veiga-da-Cunha M, Van Schaftingen E, Bommer GT. The synthesis of branched-chain fatty acids is limited by enzymatic decarboxylation of ethyl- and methylmalonyl-CoA. Biochemical Journal. 2019;476(16):2427-47.

79. Linster CL, Noel G, Stroobant V, Vertommen D, Vincent MF, Bommer GT, et al. Ethylmalonyl-CoA decarboxylase, a new enzyme involved in metabolite proofreading. Journal of biological chemistry. 2011;286(50):42992-3003.
80. Sheppard TJ, Specht DA, Barstow B. Efficiency estimates for electromicrobial production of branched-chain hydrocarbons. iScience. 2024;27(1):108773.
81. Collins T, Gerday C, Feller G. Xylanases, xylanase families and extremophilic xylanases. FEMS microbiology reviews. 2005;29(1):3-23.
82. Indiveri C, Iacobazzi V, Tonazzi A, Giangregorio N, Infantino V, Convertini P, et al. The mitochondrial carnitine/acylcarnitine carrier: function, structure and physiopathology. Molecular aspects of medicine. 2011;32(4-6):223-33.
83. Liepinsh E, Kalvinsh IY, Dambrova M, editors. The Regulation of Energy Metabolism Pathways Through L-Carnitine Homeostasis. Role of the Adipocyte in Development of Type; 2011.
84. Wang S, Huang H, Moll J, Thauer RK. NADP+ reduction with reduced ferredoxin and NADP+ reduction with NADH are coupled via an electron-bifurcating enzyme complex in Clostridium kluyveri. Journal of bacteriology. 2010;192(19):5115-23.
85. Ankri S, Mirelman D. Antimicrobial properties of allicin from garlic. Microbes and infection. 1999;1(2):125-9.
86. Martin C, Morgavi DP, Doreau M. Methane mitigation in ruminants: from microbe to the farm scale. Animal. 2010;4(3):351-65.

Table 1. Composition of diet used in the *in vitro* fermentation experiment.

Parameters	Oat hay	Pellet concentrate
Dry matter, % of DM	91.56	89.19
Crude protein,% of DM	3.55	16.20
Crude fat,% of DM	2.15	4.08
Crude fiber,% of DM	27.40	8.66
Crude ash,% of DM	5.02	6.95
Calcium, % of DM	0.09	1.22
Phosphorus, % of DM	0.09	0.65
ADF, % of DM	30.87	13.23
NDF, % of DM	54.17	31.10

Composition of diet ingredients used in the in vitro fermentation experiment. Values represent nutrient composition expressed on a dry matter (DM) basis. Abbreviations: DM = dry matter; ADF = acid detergent fiber; NDF = neutral detergent fiber.

Table 2. Comprehensive analysis of rumen fermentation parameters, methane production, and microbial population dynamics in response to garlic oil and rubber seed oil supplementation in *in vitro* batch culture systems

Parameters	Treatments								SEM	p-value
	CON	RO2	RO4	RO6	GO	GORO2	GORO4	GORO		
DMD, %	70.7^{a}	70.6^{a}	70.7^{a}	68.5^{a}	65.8^{b}	66.8^{b}	65.8^{b}	64.1^{b}	0.57	<0.001
Gas production (total), mL	129.4^{a}	131.3^{a}	128.0^{a}	127.4^{a}	113.1^{b}	112.7^{b}	115.1^{b}	112.2^{b}	1.76	<0.001
3 h, mL	34.2	34.7	33.6	33.7	32.9	32.7	33.3	32.7	0.90	0.700
6 h, mL	23.4^{a}	23.5^{a}	23.0^{ab}	22.7^{ab}	19.6^{c}	19.8^{c}	20.4^{bc}	19.7^{c}	0.57	<0.001
12 h, mL	31.2^{a}	31.6^{a}	30.6^{a}	29.8^{a}	24.5^{b}	24.5^{b}	25.1^{b}	24.5^{b}	0.55	<0.001
24 h, mL	35.9^{a}	36.7^{a}	35.9^{a}	36.4^{a}	31.2^{b}	30.9^{b}	31.4^{b}	30.6^{b}	0.68	<0.001
pH	6.31^{b}	6.30^{b}	6.30^{b}	6.30^{b}	6.35^{a}	6.35^{a}	6.34^{a}	6.34^{a}	0.01	<0.0001
Total VFA, mmol/L	65.1	64.2	63.9	65.6	58.6	60.0	59.4	60.6	1.96	0.080
Acetate, mol/100 mol	62.4^{a}	62.5^{a}	62.7^{a}	62.1^{a}	58.4^{b}	58.6^{b}	58.7^{b}	58.5^{b}	0.49	<0.001
Propionate, mol/100 mol	19.7^{b}	19.6^{b}	19.9^{b}	19.9^{b}	21.3^{a}	21.6^{a}	21.2^{a}	21.3^{a}	0.19	<0.001
Butyrate, mol/100 mol	13.5^{b}	13.6^{b}	13.3^{b}	13.8^{b}	15.9^{a}	15.4^{a}	15.6^{a}	15.8^{a}	0.23	<0.001
Valerate, mol/100 mol	1.55	1.47	1.44	1.46	1.58	1.57	1.58	1.57	0.13	0.894
Isobutyrate, mol/100 mol	1.07	1.01	0.99	0.97	0.90	0.88	0.91	0.89	0.14	0.482
Isovalerate, mol/100 mol	1.82	1.75	1.71	1.82	1.89	2.01	2.04	1.90	0.01	0.459
A:P ratio	3.17^{a}	3.19^{a}	3.16^{a}	3.12^{a}	2.74^{b}	2.72^{b}	2.77^{b}	2.74^{b}	0.04	<0.001
NH_3-N, mg/dL	22.0^{c}	21.9^{c}	22.1^{bc}	22.3^{bc}	22.2^{bc}	23.0^{abc}	24.7^{a}	24.1^{ab}	0.45	<0.001
CH_4 yield, mL	6.82	7.11	6.73	6.54	3.21	3.40	3.66	3.29	0.23	<0.001
CH_4, mL/g dDM	19.3^{a}	20.1^{a}	19.0^{a}	19.1^{a}	9.73^{b}	10.2^{b}	11.1^{b}	10.3^{b}	0.67	<0.001
Isotrichids, log_{10}, cell counts per mL of inoculum	4.83^{ab}	4.86^{ab}	4.89^{a}	4.83^{ab}	4.78^{ab}	4.72^{b}	4.76^{ab}	4.73^{ab}	0.04	0.014
Entodiniomorphs, log_{10}, counts per 1 ml	5.32^{ab}	5.34^{a}	5.27^{ab}	5.29^{ab}	5.28^{ab}	5.25^{b}	5.26^{ab}	5.22^{b}	0.02	0.018
Total protozoa, log_{10}, cell counts per mL of inoculum	5.45^{ab}	5.47^{a}	5.42^{ab}	5.42^{ab}	5.40^{abc}	5.37^{bc}	5.38^{abc}	5.34^{c}	0.02	<0.001
Total Bacteria, log_{10}, copy number/ml of culture	10.38	10.17	10.28	10.40	9.23	9.34	10.03	9.52	0.43	0.115
Total methanogens, log_{10}, copy number/ml of culture	8.38	8.40	8.44	8.75	8.72	7.90	8.06	8.65	0.30	0.903

Effects of dietary supplementation with rubber seed oil (RO2, RO4, RO6), garlic oil (GO), and their combinations (GORO2, GORO4, GORO) compared with the control (CON) on rumen fermentation parameters, methane production, and microbial population dynamics in in vitro batch culture systems. Parameters include dry matter digestibility (DMD), 3–24 hours gas production, total gas production, 3 to 24 hours gas production, volatile fatty acid (VFA) composition, acetate-to-propionate ratio (A:P), ammonia nitrogen (NH_3-N), methane (CH_4) yield and production per gram digested dry matter (dDM), and microbial counts (isotrichids, entodiniomorphs, total protozoa, total bacteria, and total methanogens). Values represent means of five independent replicates per treatment with standard error of mean (SEM). Statistical significance was assessed using one-way ANOVA and the Kruskal–Wallis test, followed by Tukey's HSD and Dunn's post-hoc pairwise comparisons. Different superscript letters within rows indicate significant differences among treatments ($p < 0.05$).

Table 3. Alpha diversity indices of rumen microbial communities under different dietary treatments demonstrate contrasting effects of garlic oil (GO) alone versus combined garlic oil-rubber seed oil (GORO) supplementation.

Parameters	Treatments			SEM	*p*-value
	CON	GO	GORO		
Chao1	1257^{a}	865^{b}	1256^{a}	13.94	0.008
Evenness	0.905^{a}	0.802^{c}	0.886^{b}	0.002	0.002
Faith's phylogenetic diversity	89.33^{a}	72.37^{b}	89.45^{a}	1.26	0.009
Shannon's diversity	9.31^{a}	7.82^{c}	9.12^{b}	0.024	0.002
Simpson's index	0.997^{a}	0.984^{c}	0.994^{b}	0.000	0.002

Inverse Simpson	303.93[a]	63.49[c]	173.44[b]	8.64	0.002
Good's coverage	0.999	0.999	0.999	0.000	0.690

Alpha diversity indices of rumen microbial communities under different dietary treatments (CON = control, GO = garlic oil, GORO = garlic oil–rubber seed oil combination). Parameters include species richness (Chao1), community evenness, phylogenetic diversity (Faith's PD), entropy-based diversity (Shannon's index), dominance-based diversity (Simpson's index and Inverse Simpson), and sequencing coverage (Good's coverage). Values represent means of five biological replicates with standard error of mean (SEM). Statistical significance was assessed using the Kruskal–Wallis test with post-hoc pairwise comparisons. Different superscript letters within rows indicate significant differences among treatments ($p < 0.05$).

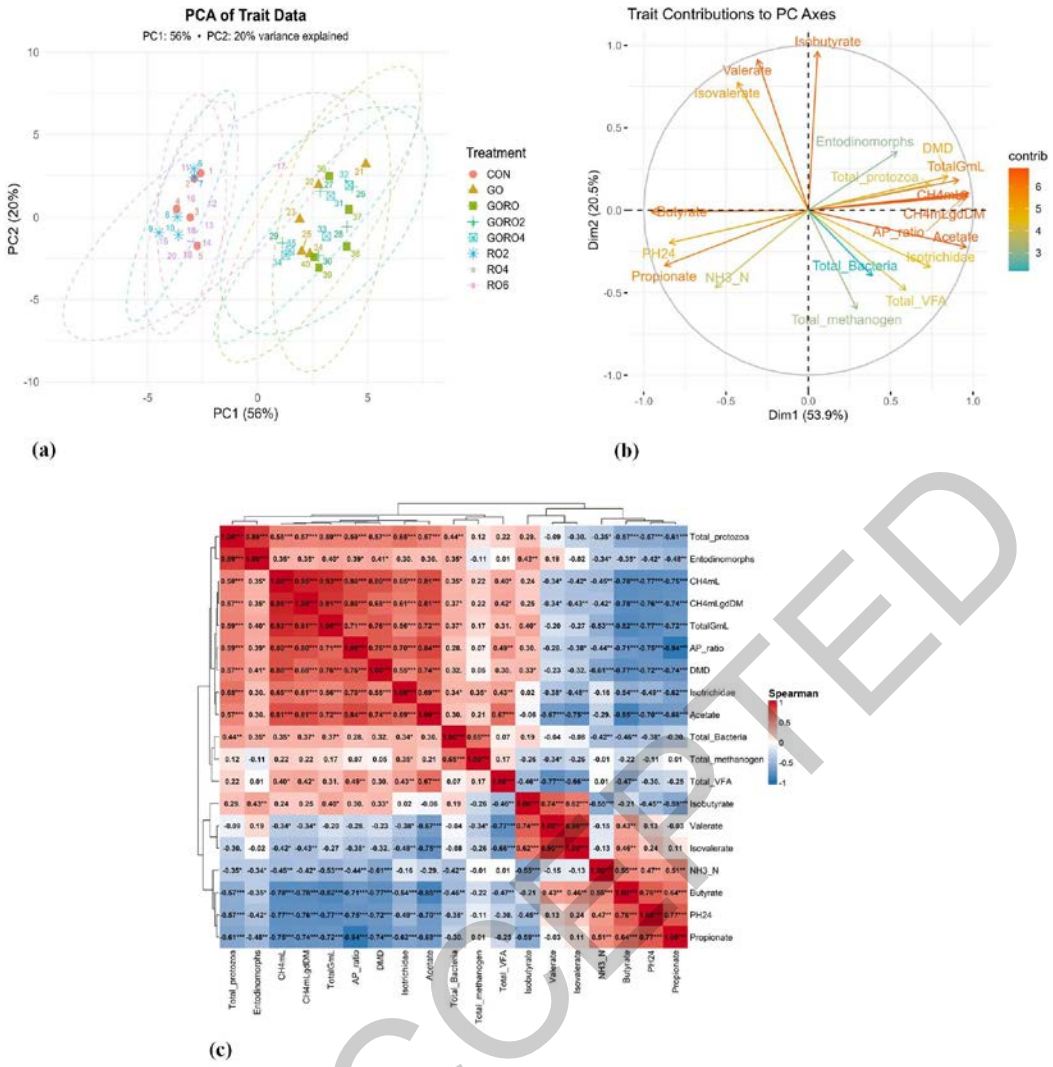

Figure 1. Integrated analysis of gas production kinetics, fermentation parameter relationships, and multivariate treatment separation.

(a) Principal component analysis (PCA) of fermentation traits: two-dimensional PCA plot displaying sample clustering based on fermentation parameters, with each point representing individual replicates colored by treatment group. Variance explained by PC1 and PC2 axes is indicated, demonstrating clear treatment separation.

(b) Fermentation parameter loading plot: PCA biplot illustrating individual fermentation trait contributions to principal components, with vector arrows indicating direction and magnitude of each parameter's influence on treatment separation.

(c) Spearman correlation matrix with hierarchical clustering: The heatmap displays pairwise Spearman correlation coefficients among variables, with hierarchical clustering applied to both rows and columns. Color intensity reflects the strength and direction of correlation (blue: negative, red: positive), and overlaid values include significance stars (*p < 0.05, **p < 0.01, ***p < 0.001). Dendrograms indicate clustering structure based on correlation distance.

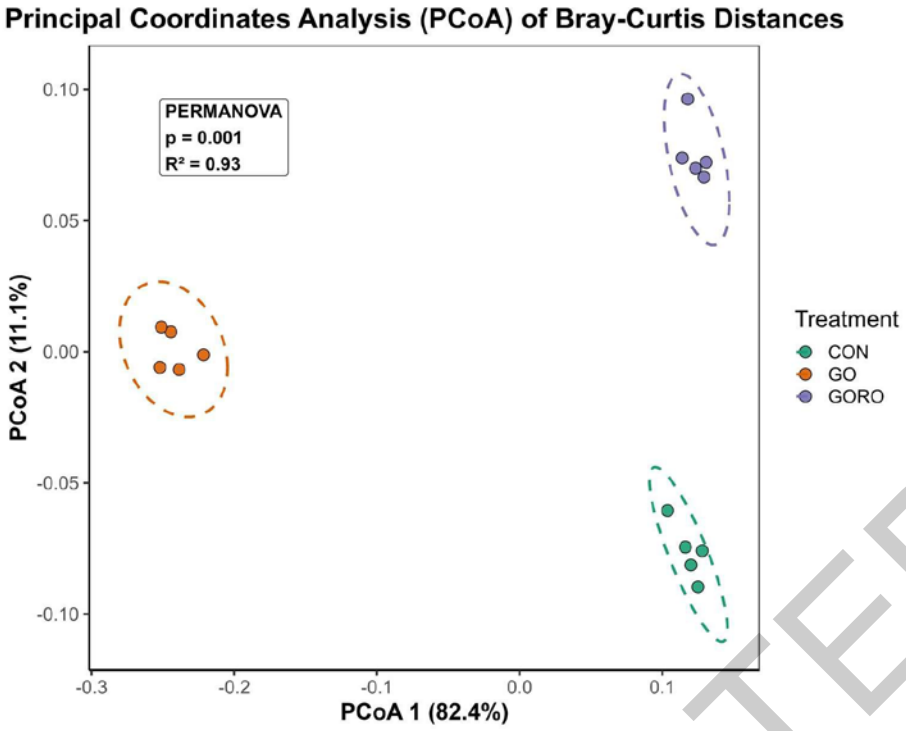

Figure 2. Microbial community analysis across dietary treatments.

Beta diversity ordination: Principal Coordinates Analysis (PCoA) based on Bray–Curtis dissimilarity at the genus level, illustrating differences in community composition among treatments. Points represent individual replicates colored by treatment group, with variance explained by the first two coordinate axes indicated. PERMANOVA results confirm significant treatment effects on microbial community structure ($p = 0.001$, $R^2 = 0.93$, stress = 7.3×10^{-5}).

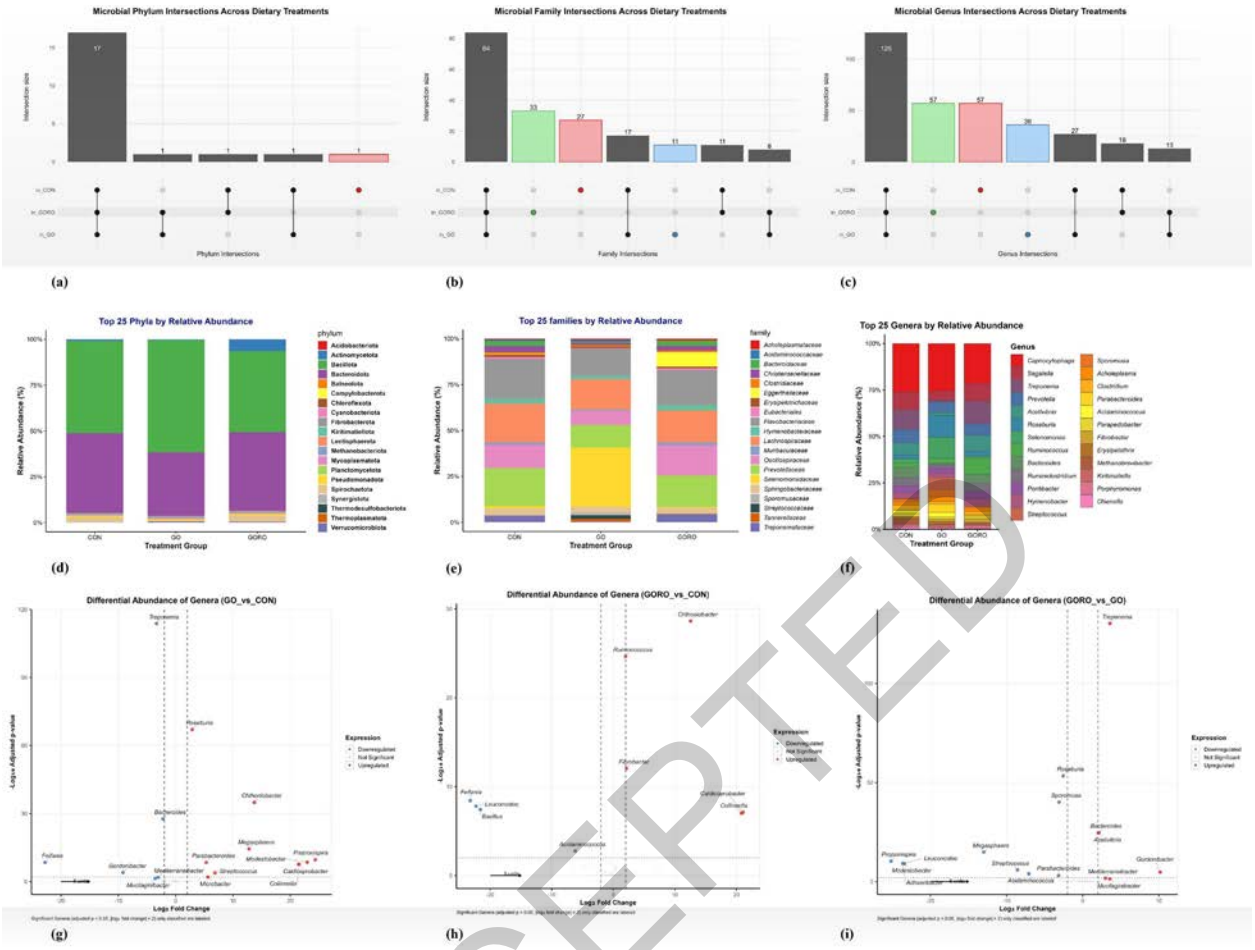

Figure 3. Comprehensive microbial community intersection analysis and differential abundance assessment. (a–c) Taxonomic intersection analysis: UpSet diagrams quantifying shared and unique microbial taxa across treatments at phylum (a), family (b), and genus (c) levels. Bar heights indicate the number of shared taxa, and connection patterns illustrate overlaps among treatment groups.
(d–f) Relative abundance profiles: stacked bar charts showing mean relative abundances of the top 25 most abundant phyla (d), families (e), and genera (f) across CON (control), GO (garlic oil), and GORO (garlic oil–rubber seed oil combination) treatments, with color-coded taxonomic groups.
(g–i) Differential abundance volcano plots: statistical comparisons of genus-level abundance changes between treatment pairs (GO vs. CON, GORO vs. CON, and GORO vs. GO). The x-axis represents $\log_2$ fold change, and the y-axis represents $-\log_{10}$(adjusted p-value). Red points indicate significantly upregulated genera, and blue points indicate significantly downregulated genera (adjusted $p < 0.05$, $|\log_2 FC| > 2.0$).

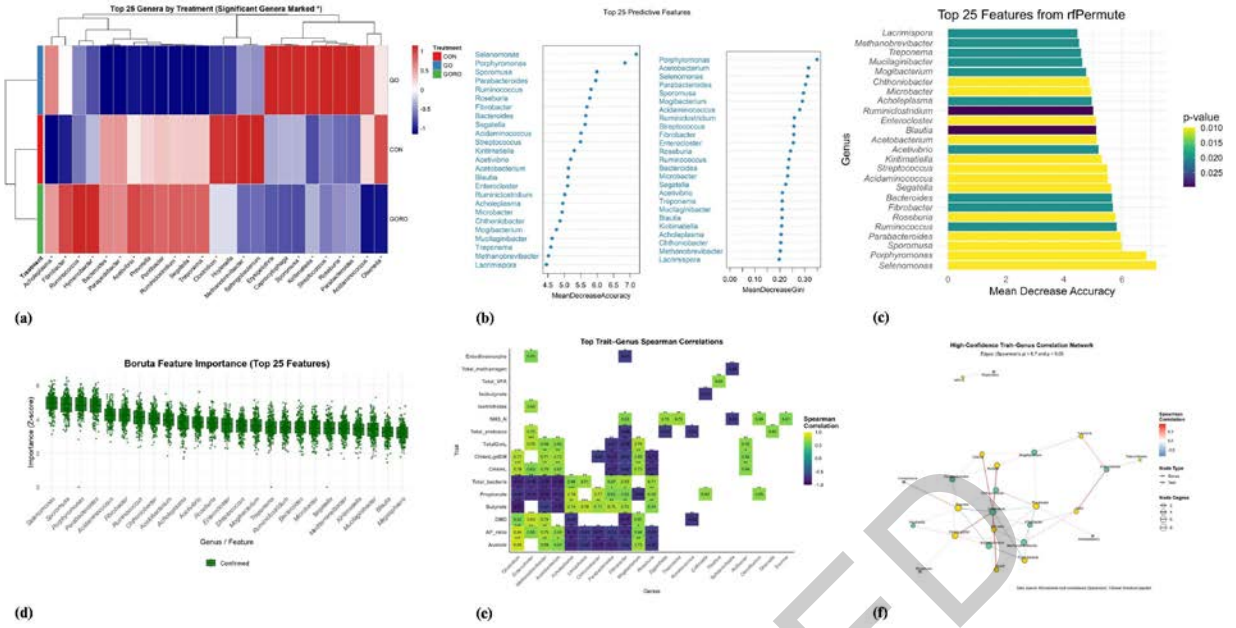

Figure 4. Advanced multivariate analysis of microbial biomarkers and fermentation parameter correlations across eight treatment groups.

Comprehensive analysis includes control (CON), garlic oil treatment (GO), and combination treatments (GORO).

(a) Heatmap of significant genera: relative abundance profiles of the top 25 genera identified as significantly different by ANOVA ($p < 0.05$), with hierarchical clustering and color intensity representing abundance levels.

(b) Random Forest biomarker identification: top 25 genera ranked by importance scores from Random Forest classification analysis, showing predictive power for treatment discrimination.

(c) Recursive feature elimination analysis: top 25 features selected by rfPermute analysis with importance rankings, identifying key microbial taxa for treatment classification.

(d) Boruta feature selection: importance scores for microbial genera determined by the Boruta algorithm, distinguishing confirmed biomarkers from shadow features.

(e) Genus–parameter correlation matrix: Spearman correlation coefficients between top microbial genera and fermentation parameters including methane production, volatile fatty acid (VFA) concentrations, and digestibility measures.

(f) High-confidence correlation network: network visualization of significant correlations ($p < 0.05$) between genera and fermentation traits, with edge thickness proportional to correlation strength and node size representing abundance.

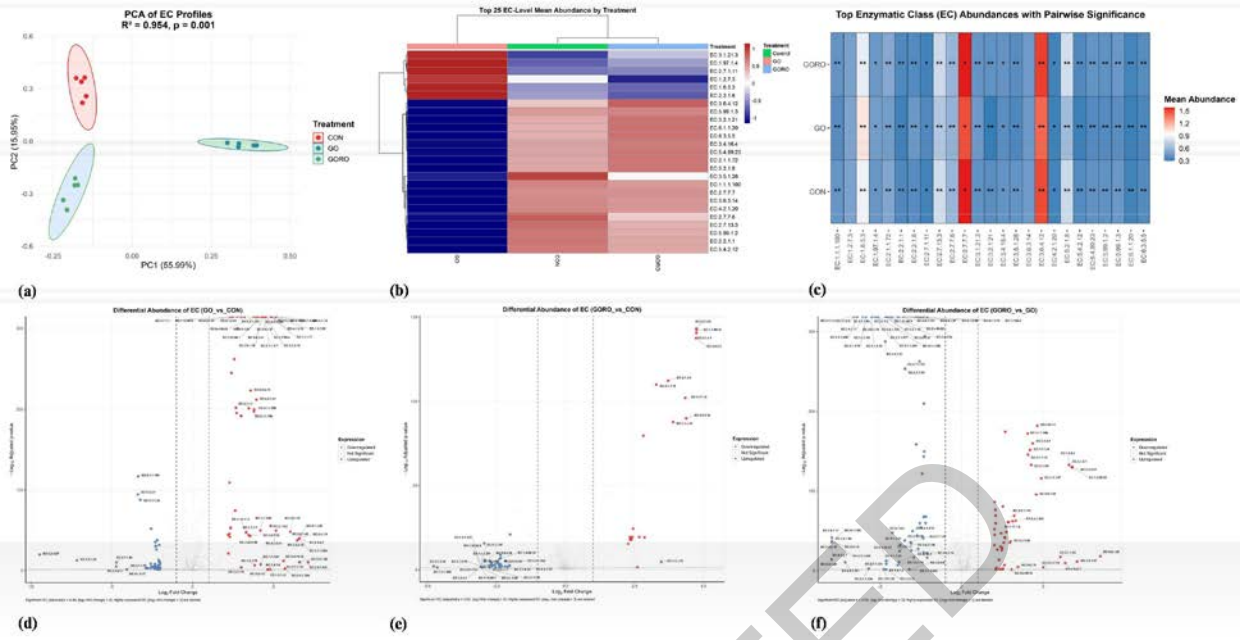

Figure 5. Enzymatic class (EC) profile analysis of rumen microbial communities under different treatments.

(a) Principal component analysis (PCA) showing distinct clustering of CON (control), GO (garlic oil), and GORO (garlic oil + rubber seed oil) treatments ($R^2 = 0.954$, $p = 0.001$).
(b) Heatmap of the top 25 EC-level mean abundances across treatments, with hierarchical clustering patterns illustrating treatment-specific functional shifts.
(c) Relative abundances of the top 25 enzymatic classes across treatments, with pairwise significance testing indicated (*$p < 0.05$, **$p < 0.01$).
(d–f) Differential function volcano plots comparing enzymatic function abundances between treatment pairs: GO vs. CON (d), GORO vs. CON (e), and GO vs. GORO (f). The x-axis represents $\log_2$ fold change in predicted enzyme abundance, and the y-axis represents $-\log_{10}$(adjusted p-value). Red points indicate significantly upregulated functions, and blue points indicate significantly downregulated functions (adjusted $p < 0.05$, $|\log_2 FC| > 3$).